TU Delft

Delft University of Technology

Document Version
Final published version

Licence
Dutch Copyright Act (Article 25fa)

Citation (APA)
Jia, Z., Ai, Z., Zhang, X., Liu, Z., & Zhong, L. (2026). Personal protective equipment increases inhalation exposure to skin-emitted bio-effluents. *Building and Environment*, *297*, Article 114602. https://doi.org/10.1016/j.buildenv.2026.114602

Important note
To cite this publication, please use the final published version (if applicable).
Please check the document version above.

Copyright
In case the licence states “Dutch Copyright Act (Article 25fa)”, this publication was made available Green Open Access via the TU Delft Institutional Repository pursuant to Dutch Copyright Act (Article 25fa, the Taverne amendment). This provision does not affect copyright ownership.
Unless copyright is transferred by contract or statute, it remains with the copyright holder.

Sharing and reuse
Other than for strictly personal use, it is not permitted to download, forward or distribute the text or part of it, without the consent of the author(s) and/or copyright holder(s), unless the work is under an open content license such as Creative Commons.

Takedown policy
Please contact us and provide details if you believe this document breaches copyrights.
We will remove access to the work immediately and investigate your claim.

This work is downloaded from Delft University of Technology.

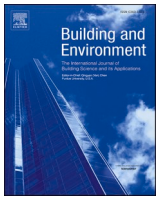
Building and Environment 297 (2026) 114602



Contents lists available at ScienceDirect

Building and Environment

journal homepage: www.elsevier.com/locate/buildenv





Personal protective equipment increases inhalation exposure to skin-emitted bio-effluents

Zhongjian Jia [a,b,c], Zhengtao Ai [a,b,*], Xiaochen Zhang [a,b], Zhengxuan Liu [d], Lexuan Zhong [c]

[a] Department of Building Environment and Energy, College of Civil Engineering, Hunan University, Changsha, Hunan, China
[b] National Center for International Research Collaboration in Building Safety and Environment, Hunan University, Changsha, Hunan, China
[c] Department of Mechanical Engineering, University of Alberta, 9211-116 Street NW, Edmonton, Alberta, T6G 1H9, Canada
[d] Faculty of Architecture and the Built Environment, Delft University of Technology, Delft, the Netherlands

ARTICLE INFO

Keywords:
Face mask
Protective clothing
Skin bio-effluents
Inhalation exposure
CFD

ABSTRACT

Personal protective equipment (PPE) restricts the dilution of skin-emitted bio-effluents, which may lead to pollutant accumulation in the breathing zone and thus intensify inhalation exposure of the wearer. This study quantifies the inhalation exposure risk caused by skin-emitted bio-effluents under PPE using ethyl acetate as a tracer combined with a mannequin method. The distributions of thermal-fluid parameters were predicted using computational fluid dynamics. The dispersion of skin bio-effluents was visualized, and the influence of breathing organ, pulmonary ventilation rate, bio-effluent emission rate, and emission location on inhalation exposure was examined. Wearing protective clothing increased the average air temperature and air velocity in the breathing zone by 0.9 °C and 0.09 m/s, respectively, compared with conditions without PPE. The neck and cuffs served as the dominant pathways for leakage of skin-emitted bio-effluents. Protective clothing led to higher inhalation exposure to skin bio-effluents than no PPE, with nasal breathing receiving slightly higher inhalation concentrations than oral breathing. When pulmonary ventilation rate increased from 6 to 9 L/minute under a standing posture and oral breathing, the relative inhalation concentration and the relative exposure index increased by 30.6% and 17.8%, respectively. Inhalation exposure also rose sharply when emission rates exceeded 700 μg $h^{-1}p^{-1}$. Emission location strongly affected inhalation exposure. Bio-effluents emitted from the groin resulted in substantially higher inhalation exposure than those emitted from the armpit. These findings would enhance the scientific understanding of human-related bio-effluents and further support the rational improvement of PPE design and the effective control of human-related pollutants.

1. Introduction

Personal protective equipment (PPE), such as face masks and protective clothing, is widely applied in health care [1,2], biopharmaceutical manufacturing [3], electronic product manufacturing [3], and other advanced manufacturing industries. In controlled environments, such as operating rooms or clean rooms, PPE protects both wearers and nearby personnel or sensitive products (e.g., drugs and microchips) by preventing inward leakage of external pollutants and reducing outward leakage of self-generated bio-effluents, including bacteria, moisture, and other biological emissions [4].

Despite these benefits, increasing attention has been paid to the potential adverse effects of PPE use. Respiratory-related problems have been widely reported among PPE users [5]. By restricting air exchange, PPE could intensify inhalation exposure to self-exhaled bio-effluents, contributing to dizziness [6], elevated heart rate [7], and headaches [8,9], deoxygenation, and hypercabia [10]. In addition to breath, human skin also acts as an essential source of human-related bio-effluents. As a result of metabolic processes, human skin continuously generates moisture, particles, and a wide range of biological compounds, particularly volatile organic compounds (VOCs). Ethyl acetate, acetic acid, acetone, 2-Phenyl-2-propanol, decanal, and nonanal were the most significant contributors to skin emissions [11–14]. Among skin-emitted VOC compound groups, alcohols, aldehydes, and ketones contributed the most to the emissions [11–15]. These emissions are spatially nonuniform across the human body, with the oral cavity, armpit, groin, head, and feet identified as dominant sources [16]. Hundreds of VOCs have been detected in skin secretions [17], with reported emission rates

* Corresponding author.
E-mail address: zhengtaoai@hnu.edu.cn (Z. Ai).

https://doi.org/10.1016/j.buildenv.2026.114602
Received 17 January 2026; Received in revised form 13 March 2026; Accepted 9 April 2026
Available online 9 April 2026
0360-1323/© 2026 Elsevier Ltd. All rights are reserved, including those for text and data mining, AI training, and similar technologies.

ranging from 701.4 to 4450 μg h^{-1} [11,14,18], depending on environmental conditions and personal factors, such as oxidant levels, air temperature, relative humidity, long clothing, etc. [11,19,20].

Complex airflow interactions, including breathing-induced flow, thermal convective flow, and background ventilation flow, shape exposure levels near the human body [21]. Protective clothing slows down the dispersion of skin-generated bio-effluents while leaving openings at the neck and cuffs. Temperature differences between the body and the surrounding air generate upward airflow, and body movement induces pressure variations that pump bio-effluents through these openings. As a result, the breathing zone becomes a major pathway for skin-emitted bio-effluents to leak. While some bio-effluents disperse into the surrounding environment, others remain near the mouth/nose and are then inhaled by the wearer.

Previous studies have examined exposure to skin-generated bio-effluents under ordinary clothing conditions (Table 1), showing that airflow interactions strongly influence concentrations in inhaled air in the breathing zone. Our earlier work [22] demonstrated that wearing a face shield markedly increases the inhaled fraction of skin-emitted bio-effluents. Protective clothing, due to its low breathability and moisture permeability, further alters this process by allowing bio-effluents to accumulate inside the clothing for extended periods. PPE users often engage in moderate to high physical activity, which increases metabolic rates and, consequently, the emission of skin-generated bio-effluents. The combination of reduced dilution and increased emission rates raises the potential for inhalation exposure. Additionally, previous studies [23–25] have indicated that reaction products formed from human-emitted compounds, including secondary organic aerosols and ozone-skin oil byproducts, pose potential risks to the respiratory system and eyes, and may also increase susceptibility to illness [26–28]. VOCs are also a major source of body odor, which can stimulate the sensory system. Dermally-emitted pollutants have a higher odor intensity compared to pollutants in exhaled air and may negatively impact occupants' health, well-being, and productivity [9]. Despite these health concerns, inhalation exposure to skin-generated bio-effluents under PPE use has not been systematically evaluated, and the effectiveness of PPE in controlling these bio-effluents remains unclear.

Table 1
Assessment of inhalation exposure to self-generated pollutants.

Emission location	with/without PPE	Main findings	Reference
Armpit and groin	Without	The interaction between exhaled airflow and the convective boundary layer increases inhalation exposure to self-generated contaminants, particularly when the pollution source is located near the breathing zone.	Bivolarova (2017) [21]
Breath	Without	Approximately 16.2% to 17.2% of exhaled air is inhaled.	Zhu (2005) [29]
Breath	Without	The rebreathing rate is less than 1%, but the overall rebreathing rate of exhaled gas may be higher due to increasing background concentrations.	Kuga (2022) [30]
Breath	Without	The re-inhalation rate under the four breathing patterns ranges from 0.3% to 1.0%.	Zong (2023) [31]
Breath	Filter-type protective mask	The molar fraction of exhaled CO_2 was 4.88%, while the flow-weighted molar fraction of inhaled CO_2 was approximately 2.09%, indicating that about 43% of exhaled carbon dioxide was re-inhaled.	Lei and Yang (2014) [32]
Breath/ armoit/ groin	Face shield	The inhalation rate of autologous contaminants from different body regions ranges from 0.17% to 6.95%.	Jia (2022) [22]
Breath	Face shield/ mask	For users of respiratory protective equipment, approximately 37% to 60% of exhaled contaminants are re-inhaled.	Jia (2024) [15]
Breath	Mask	The rate of rebreathing self-exhaled pollutants ranges from 29% to 54%.	Jia (2024) [33]

To address these gaps, this study developed a refined three-dimensional computational thermal manikin with a face mask and protective clothing. Computational fluid dynamics (CFD) coupled with a species transport model was used to investigate the dispersion and accumulation of bio-effluents inside the PPE. The study analyzed airflow, pressure, air temperature, relative humidity, and bio-effluent concentration in the breathing zone. The effect of breathing organ, pulmonary ventilation rate, bio-effluent emission rate, and emission location was also examined. These findings aim to enhance scientific understanding of the dispersion of exposure risks of human-related bio-effluents and to support the rational improvement of PPE design.

2. Methodology

2.1. CFD simulation

2.1.1. Computational geometry and numerical setup

A full-scale test room with dimensions of 4 m × 3 m × 2.6 m was modelled, ventilated with displacement ventilation, commonly used in cleanrooms, operating rooms, and other PPE-use environments. A supply inlet (0.4 m × 0.2 m) and an exhaust outlet (0.4 m × 0.2 m) were installed on the same wall. The inlet was located near the floor, while the outlet was positioned near the ceiling, as shown in Fig. 1(a). Fresh air entered the room at a speed of 0.2 m/s, with a temperature of 22 °C and relative humidity of 50%. Details on boundary conditions are shown in Table 2.

A three-dimensional computational thermal model (CTM) wearing PPE was located at the center of the room, facing the wall with a supply inlet and exhaust outlet. Different skin temperatures were assigned to individual body parts with a range of 30.5–32.8 °C to reflect physiological variations [22], with the thermoregulation model assuming steady-state temperatures. The CTM breathed through either the mouth or the nose, and the exhaled air was set to 32.7 °C with a relative humidity of 90%. Pulmonary ventilation rate ranged from 6 to 9 L/min, representing light-level activities [34,35]. A complete assumed breathing cycle was imposed in the model. Each cycle included exhalation (2.5 s), break (1.0 s), and inhalation (2.5 s) [15,22,36], and the airflow pattern is shown in Fig. 1(b).

The PPE considered in the present study included a face mask and protective clothing. A cup-type face mask was modeled to represent high-protection masks, such as N95 and KN95, as shown in Fig. 1(d). The face mask geometry was simplified based on its shape during actual use. It closely fitted the most facial regions, while a semi-elliptical gap remained near the nose bridge. The width of this gap was less than 10 mm. The thickness of the face mask was set to 1 mm for all simulations, which was consistent with those adopted in previous studies [37,38]. Airflow through the mask was simulated using a scientifically validated porous media model with the viscous resistance coefficient (4.34×10^8) and inertia resistance coefficient (5.34×10^5), and the detailed descriptions can be found in our previous studies [15,36].

Protective clothing was modeled to closely match its actual shape during use, as shown in Fig. 1(c). It covered the human body except for the face, hands, and feet, leaving openings at these locations. The maximum distances between the clothing edge and the skin were approximately 10 mm at the face, wrists, and 15 mm at the ankles, allowing air exchange between the interior and the exterior. The air gap between the protective clothing and the body considerably affects heat transfer, airflow, and pollutant transport. Reported air gap thickness

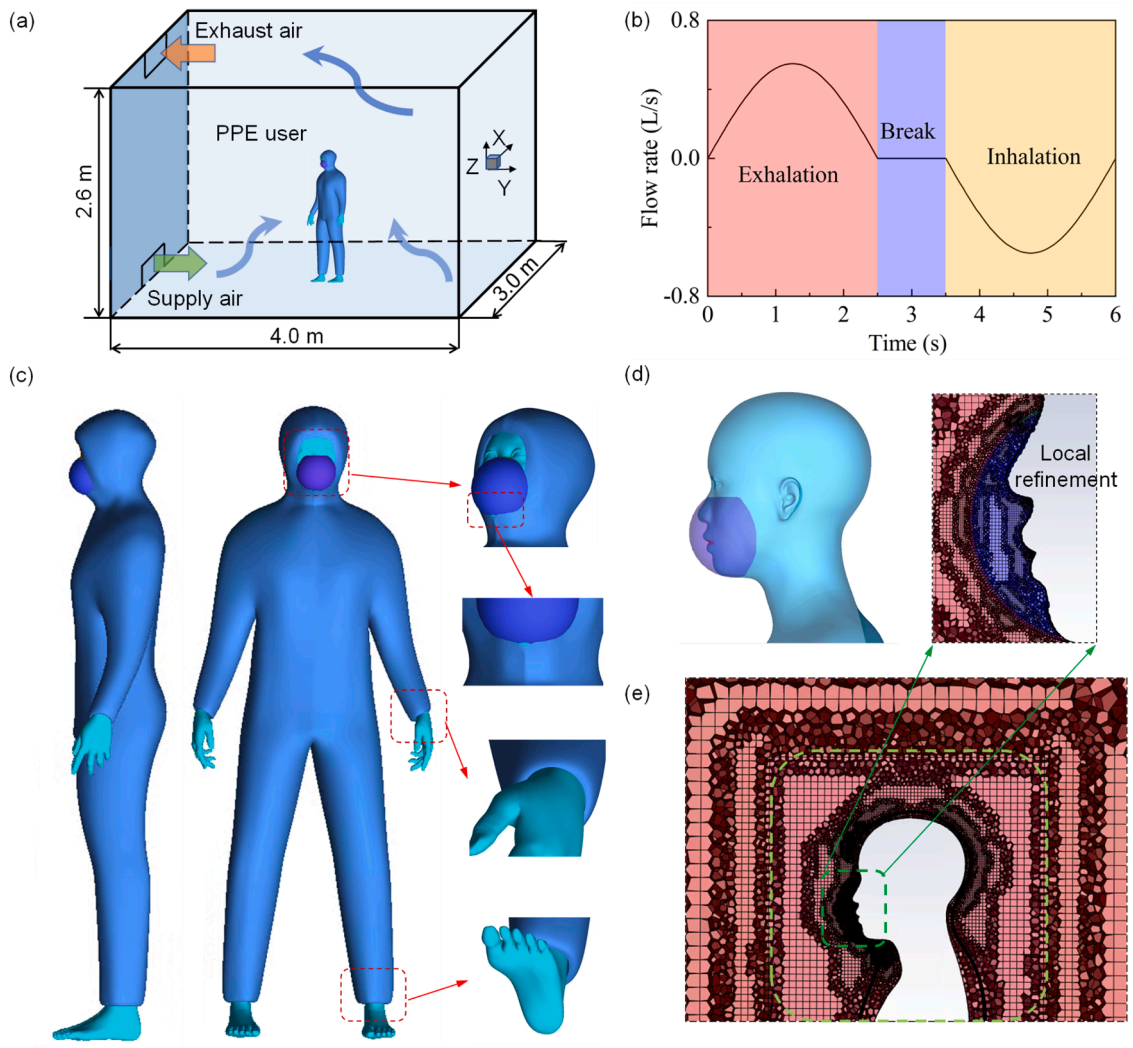


Fig. 1. Geometric model and grid division: (a) test room, (b) breathing airflow pattern [33], (c) manikin wearing PPE, (d) head wearing an N95 mask, and (e) local grids in the breathing zone. Note: The colors in Fig. 1(e) represent different computational domains.

Table 2
Boundary conditions for CFD simulation.

Boundaries	Velocity (m/s)	Temperature (°C)
Air inlet	$v = 0.2$	$T = 22$
Air outlet	$\frac{\partial v}{\partial n}=0$	$T = 30$
Wall	$\frac{\partial v}{\partial n}=0$	$\frac{\partial T}{\partial n}=0$
Body	$\frac{\partial v}{\partial n}=0$	T= constant (30.5–32.8)
Mouth	Profiles in Fig. 1(b)	$T = 32.7$

varies across studies, ranging from 5 to 37 mm [39,40]. In this study, average air gap thicknesses were specified for major body regions, including about 12 mm at the head, 21 mm at the arms, 28 mm at the chest, 10 mm at the back, and 25 mm at the legs, which are consistent with previous experimental investigations [40–43]. This agreement supports the realism of the modeled clothing configurations.

Bio-effluents generated by different body regions were considered. The groin and armpit were selected as emission locations due to their high emission intensities [22,44]. Ethyl acetate ($C_4H_8O_2$) was used as a tracer for skin-emitted VOCs, primarily to evaluate relative inhalation fraction and exposure dynamics, rather than to assess the risk of a specific chemical, as commonly done in building and environmental research. It was selected because it exhibits one of the highest emission rates among skin-related VOCs [12,18]. According to the experimental results by Sun et al. [18], the emitted rate of bio-effluents (VOCs) was determined to be 701.4 μg h^{-1} in most cases. The initial concentration of ethyl acetate on the body surface was set to 0, and zero diffusion flux boundary conditions were applied at all body locations except for the source regions (mass inlets at groin and armpit). This setup ensures that the scalar spreads only from the designated source, while other body surfaces do not contribute to scalar flux.

2.1.2. Grid generation

A hybrid grid composed of polyhedron and hexahedron elements was employed. Regular regions were filled by ortho-hexahedra, while irregular regions were filled with polyhedral grids [45]. Local mesh refinement was applied around the human body and protective clothing, with a maximum cell size of 15 mm. The grid near the face mask was further refined, with a maximum cell size of 1.5 mm (Fig. 1(e)). Five inflation layers were added adjacent to the solid surfaces, with the first layer near the surface at a height of 0.1 mm to resolve the flow profile within the viscous sublayer. The narrow gap between the face and the face mask was further refined. In this region, the maximum cell size was also restricted to 1.5 mm to ensure numerical stability. Mesh quality was carefully controlled throughout the domain. The maximum skewness of all grid elements remained below 0.9, meeting the CFD benchmark

criteria and recommended guidelines.

Grid independence was evaluated using four cell densities (1.79 million, 2.31 million, 3.68 million, and 4.44 million cells). These cases were tested independently to determine an optimal balance between accuracy and computational cost. Air speed, air temperature, and relative concentration of CO_2 (C/C_0, where C_0 refers to the concentration of CO_2 in exhaled air) at a line located 0.1 m in front of the human body were extracted and compared for grid validation. Comparisons between the 1.79 and 2.31 million cell grids showed large deviations, with average relative deviations for air speed, air temperature, and, C/C_0 of 32.3%, 0.2%, and 59.4%, respectively, as shown in Fig. 2. Increasing the grid density from 2.31 to 3.68 million cells reduced these deviations to −4.0% for air speed, −0.1% for air temperature, and 39.4% for C/C_0. Further refinement to 4.44 million cells resulted in only minor changes, with average relative deviations of 0.5% for air speed, −0.2% for air temperature, and 14.4% for C/C_0. The concentration field is more sensitive to grid resolution, which may be due to small differences in airflow or thermal gradients being amplified through advection and diffusion, leading to larger variations in predicted concentrations compared to velocity or temperature. Considering both numerical accuracy and computational cost, the grid with 3.68 million cells was selected for the final simulations.

2.1.3. Solver setting

The shear stress transport (SST) k-ω model was used to predict airflow, as it has reliable performance in predicting airflow around a face mask at acceptable computational cost [36]. The second-order upwind discretization scheme was adopted for the convection and diffusion terms in the momentum, energy, and species equations. The "PRESTO" scheme was used to discretize the pressure terms. The Pressure-Implicit with Splitting of Operators (PISO) algorithm was used for the pressure–velocity coupling. The second-order implicit scheme was used to discretize the time term. The time step was fixed at 0.01 s to accurately capture transient breathing, which has been demonstrated to be reasonable [36] (Fig. 3). Exhaled and ambient air were treated as incompressible, ideal gases to simulate the buoyancy effect caused by temperature differences [46]. Convergence of the solution was checked using a convergence criterion of 10^{-6} for energy and 10^{-5} for the rest of the parameters.

The governing equations for scalar transport can be expressed as:

$$\frac{\partial}{\partial t}(\rho Y C_i) + \nabla\cdot(\rho \vec{v} C_i) = \nabla\cdot\left[\left(\rho D_{i,m} + \frac{\mu_t}{Sc_t}\right)\nabla C_i\right] \quad (1)$$

where, C_i is the mass concentration of the ith species, %; ρ is the density, kg/m^3; t is the time, s; $\vec{v}$ is the fluid velocity, m/s; $D_{i,m}$ is the mass diffusion coefficient for the ith species in the mixture; μ_t is the turbulent viscosity; Sc_t is the turbulent Schmidt number.

2.1.4. Model validation

To validate the accuracy of CFD simulations in predicting the dispersion of the contaminant inside the protective clothing, climate chamber experiments were conducted using a thermal manikin. The experiments were performed in a full-scale climatic chamber with the dimensions of 5.7 m × 3.4 m × 2.6 m. The wall of the chamber was made of insulating materials to minimize external heat exchange. A mixing ventilation mode was employed, and three supply inlets (0.25 m × 0.25 m) were located at the upper part of the front wall, while three exhaust outlets (0.25 m × 0.25 m) were located at the lower part of the same wall. The chamber was supplied with 100% fresh air at an air change rate of 6 times per hour.

A realistically shaped thermal manikin was seated at the center of the chamber, facing the wall with exhaust outlets, located 1.5 m away from the wall. The manikin's height was 1.45 m, with the mouth located at 1.25 m above the floor. The manikin consisted of 17 independently controlled body segments. Surface temperatures were individually regulated by a computer program and ranged from 31 °C to 34 °C during experiments. Respiratory patterns followed a sinusoidal pattern with a pulmonary ventilation rate of 9 L/min [47]. The manikin wore full-body personal protective clothing and a face mask throughout the tests. A tracer gas generator connected to a carbon dioxide (CO_2) cylinder simulated the emission of a contaminant released from the groin. CO_2 concentrations were measured at multiple locations. Sensors were placed both inside the protective clothing at the chest and outside the mask near the breathing zone, located 3 cm from the mouth. Additionally, CO_2 concentrations in fresh air outdoors were recorded to eliminate background concentration interference from the measured results. During the experiment, the air temperature and relative humidity were maintained at 22 °C (±0.5 °C) and 40% (±2%), respectively. The experiment cases were reproduced using CFD simulations.

Simulation results generally agreed with experimental results, with maximum relative deviations of 15%, as shown in Fig. 4. Discrepancies

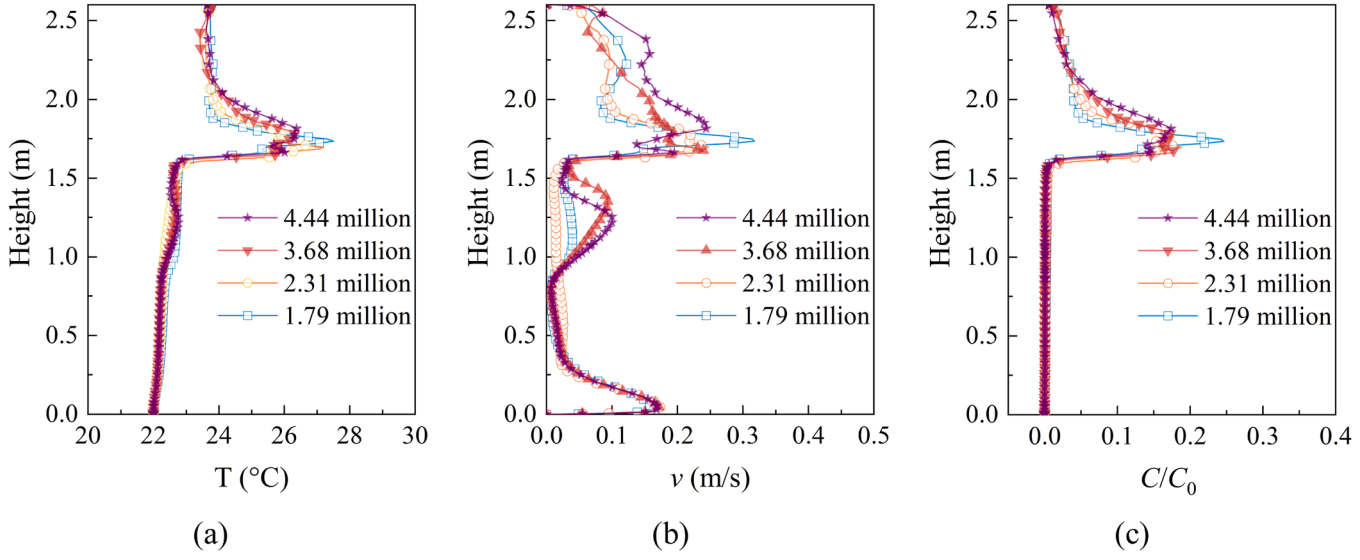


Fig. 2. Grid independence test: (a) air temperature in front of the human, (b) air speed in front of the human, and (c) relative CO_2 concentration (C/C_0, C_0 is the CO_2 concentration at the mouth) in front of the human.

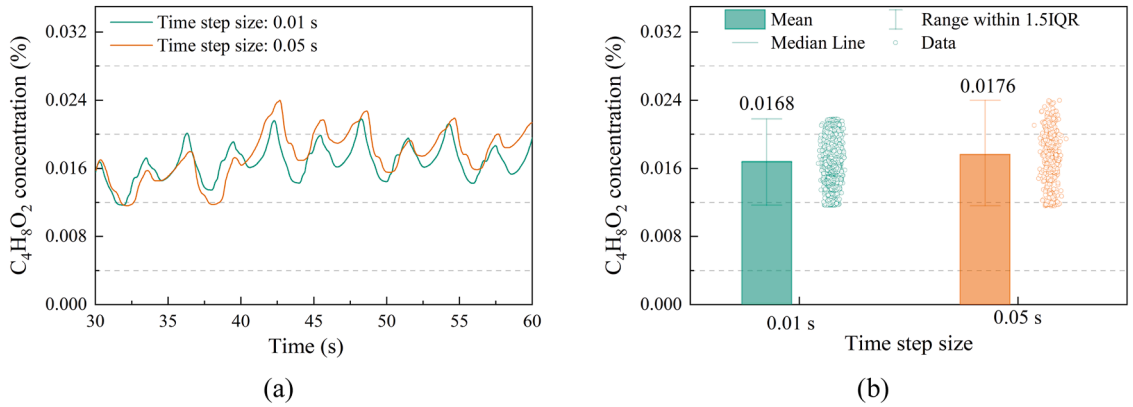


Fig. 3. Time step size independence test: (a) relative $C_4H_8O_2$ concentration (C/C_0, C_0 is the $C_4H_8O_2$ concentration at the source) over time in front of the human face, and (b) bar chart of relative $C_4H_8O_2$ concentration in front of the human face during 30–60 s.

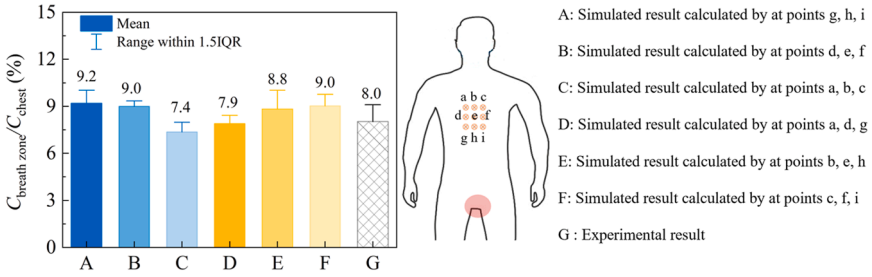


Fig. 4. Spatial distribution of bio-effluents emitted from the body surface compared with experimental results.

mainly arose from the differences in manikin geometry, air gap inside the protective clothing, and the material of the protective clothing. The CFD approach in predicting airflow fields nearby human without PPE was also validated in another study [15]. In addition, the CFD approach for airflow and bio-effluents' dispersion through a face mask has been described in detail and validated scientifically in our previous study [36].

Table 3 lists the simulated cases with different breathing organs, pulmonary ventilation rates, emission rates, and source locations under different PPE conditions. Cases 1 and 2 were designed to reveal the influence of breathing organ; Cases 1 and 3–5 were used to reveal the influence of breathing rate; Cases 1, 6, and 7 were designed to reveal the influence of emission rate; and Cases 1 and 8 were used to reveal the influence of source location.

Table 3
List of tested cases with different breathing organs, pulmonary ventilation rates, emission rates, and source locations under different PPE conditions.

Case	Breathing organ	Pulmonary ventilation rate (L/min)	Emission rate (Kg/s)	Source location	PPE
1	Mouth	6	1.95×10^{-10}	Groin	N95+clothes; N95; baseline
2	Nose	6	1.95×10^{-10}	Groin	N95+clothes; N95; baseline
3	Mouth	7	1.95×10^{-10}	Groin	N95+clothes; N95; baseline
4	Mouth	8	1.95×10^{-10}	Groin	N95+clothes; N95; baseline
5	Mouth	9	1.95×10^{-10}	Groin	N95+clothes; N95; baseline
6	Mouth	6	1.95×10^{-9}	Groin	N95+clothes; N95; baseline
7	Mouth	6	1.95×10^{-11}	Groin	N95+clothes; N95; baseline
8	Mouth	6	1.95×10^{-10}	Armpit	N95+clothes; N95; baseline

2.1.5. Data analysis

(1) Microenvironment

To evaluate the microenvironment in the breathing zone, thermo-fluid parameters (static pressure, air speed, air temperature, relative humidity, and relative $C_4H_8O_2$ concentration) outside the face mask were monitored. A semi-ellipsoidal field with a radius (R) of 7 cm around the mouth was defined, as shown in Fig. 5.

(2) Inhalation exposure

The research perspective focuses on the ventilation effectiveness of the system or the exposure risk of individuals [48]. The ventilation effectiveness was evaluated by indicators, such as ventilation effectiveness (ε_v) [49], personal exposure effectiveness (PEE) [49], and pollutant exposure reduction (PER) [50]. The exposure risk of individuals was evaluated by indicators, such as the exposure index ($\overline{\varepsilon_i}$) [22,51], protection factor (PF), normalized inhalation concentration (C^*) [21], and inhalation fraction (IF) [52,53].

$$\varepsilon_v = \frac{C_e - C_s}{C_i - C_s} \tag{2}$$

$$PEE = \frac{C_{i,o} - C_i}{C_{i,o} - C_s} \tag{3}$$

$$PER = \frac{C_a - C_i}{C_a - C_s} \tag{4}$$

$$\overline{\varepsilon_i} = \frac{C_i - C_s}{C_e - C_s} \tag{5}$$

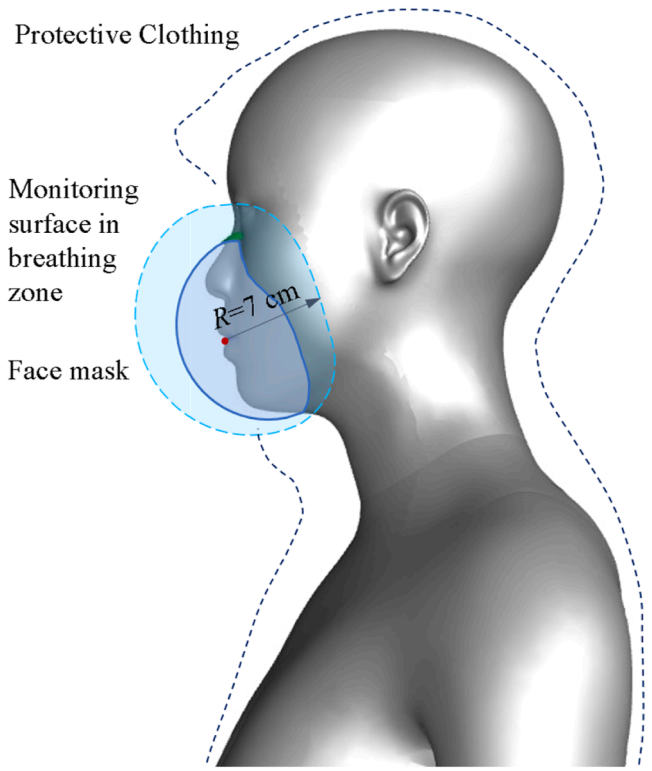


Fig. 5. The region for the determination of the thermo-fluid parameters in the breathing zone.

$$PF = \frac{C_a}{C_i} \tag{6}$$

$$C^* = \frac{C_i}{C_0} \tag{7}$$

$$IF = \frac{M_i}{M_0} \tag{8}$$

where, C_e is the pollutant concentration at the exhaust duct; $C_s$is the pollutant concentration at the supply duct; C_i is pollutant concentration at the inhalation zone (or inhaled air); $C_a$is pollutant concentration in ambient air (air exhaust concentration can be regarded as the ambient concentration); $C_{i,o}$ is pollutant concentration at the inhalation zone (or inhaled air) without protective ventilation; M_i is the pollutant mass exposed to the occupant; C_o is the pollutant concentration at a source or a polluting occupant; M_o is the pollutant mass emitted from a source or a polluting occupant.

To quantify the impact of PPE on exposure to self-generated bio-effluents, a new evaluation index, namely the relative inhalation exposure (RIE) index (ε^*), was introduced. This index compares inhalation exposure caused by PPE use. More than 1 of ε^*indicates that PPE use intensifies the inhalation exposure to self-generated bio-effluents. Unlike existing exposure indices, the RIE index directly evaluates the relative change in inhalation exposure between conditions with and without PPE. The RIE index is calculated as:

$$\varepsilon^* = \frac{C_{\text{i,with PPE}} - C_s}{C_{\text{i,without PPE}} - C_s} \tag{9}$$

where, $C_{\text{i,with PPE}}$ is the volume-averaged concentration of bio-effluents in inhaled air with PPE, C_s is the concentration of bio-effluents at the supply opening (inlet), and $C_{\text{i,without PPE}}$ is the volume-averaged concentration of bio-effluents in the inhaled air without PPE. The subtraction of the supply concentration (C_s) removes the contribution of background ventilation air and isolates the increment in inhaled concentration caused by skin-emitted bio-effluents. This treatment allows the index to highlight the additional exposure attributable to PPE-induced accumulation rather than background air supplied by the ventilation system.

3. Results

3.1. Thermo-fluid conditions in the breathing zone

3.1.1. Temporal distribution characteristics

Fig. 6 presents the time series of various thermal-fluid parameters in the breathing zone of PPE users. Wearing a face mask reduced airflow velocity in the breathing zone. However, protective clothing increased air speed substantially, raising the average from 0.04 m/s to 0.13 m/s. This increase is mainly attributed to the buoyancy-driven airflow generated inside the protective clothing. As the body continuously releases heat, the air inside the clothing warms and rises along the body surface, eventually exiting near the head region and interacting with the breathing zone. The relatively stronger upward flow near the forehead contributes to a higher spatially averaged velocity in the breathing zone. This indicates that protective clothing alters the airflow in the breathing zone, potentially affecting the dispersion of skin-emitted bio-effluents. Additionally, pressure in the breathing zone changed after wearing protective clothing. The average pressure showed a noticeable variation compared with the unclothed use. In contrast, when only an N95 mask was worn, the average pressure in the breathing zone did not show an obvious difference from the no-PPE condition because the monitoring surface was defined outside the mask and the reported value represents the spatially averaged pressure. Although a local pressure drop exists across the mask filter, it is confined near the mask interface and becomes less apparent after spatial averaging. This further emphasizes the strong influence of protective clothing on the local microenvironment. Protective clothing also elevated the air temperature in the breathing zone. When protective clothing was worn, the average air temperature in the breathing zone increased by 0.9 °C, primarily due to heat dissipating from the wearer's neck into the breathing zone. It is important to note that although absolute humidity increases in the breathing zone, the elevated air temperature further lowers its relative humidity.

Protective clothing greatly increased the accumulation of skin-emitted bio-effluents in the breathing zone. The relative concentration of bio-effluents in the breathing zone increased from 0.0033% to 0.0176%, indicating a potential increased inhalation exposure risk. To further clarify internal transport processes, contaminant concentrations were monitored inside the protective clothing at different heights, as shown in Fig. 6(f). Overall, the relative concentration of bio-effluents near the skin surface inside the protective clothing gradually decreased with increasing distance (height) from the emission source. This vertical gradient reflects upward transport along the body surface. Furthermore, the temporal evolution of bio-effluent concentration showed two distinct phases. An initial growth phase occurred immediately after emission, followed by a stable phase after 14 s.

3.1.2. Spatial distribution characteristics

To better explore the transport mechanism of bio-effluents from the body surface, spatial distributions of microenvironment parameters at 59 s were extracted, as shown in Fig. 7. A marked pressure difference formed between the interior and exterior of the protective clothing. This pressure gradient promoted outward transport of bio-effluents from the suit's interior toward the breathing zone. Protective clothing slightly reduced airflow around the periphery of the body (outside the clothing) by impeding heat transfer and diminishing the thermal plume. The airflow patterns near the face also changed, affecting contaminant transport. Wearing protective clothing led to a significant increase in air temperature near the body surface and raised the relative humidity inside the clothing from 50% to 70%, which may cause thermal

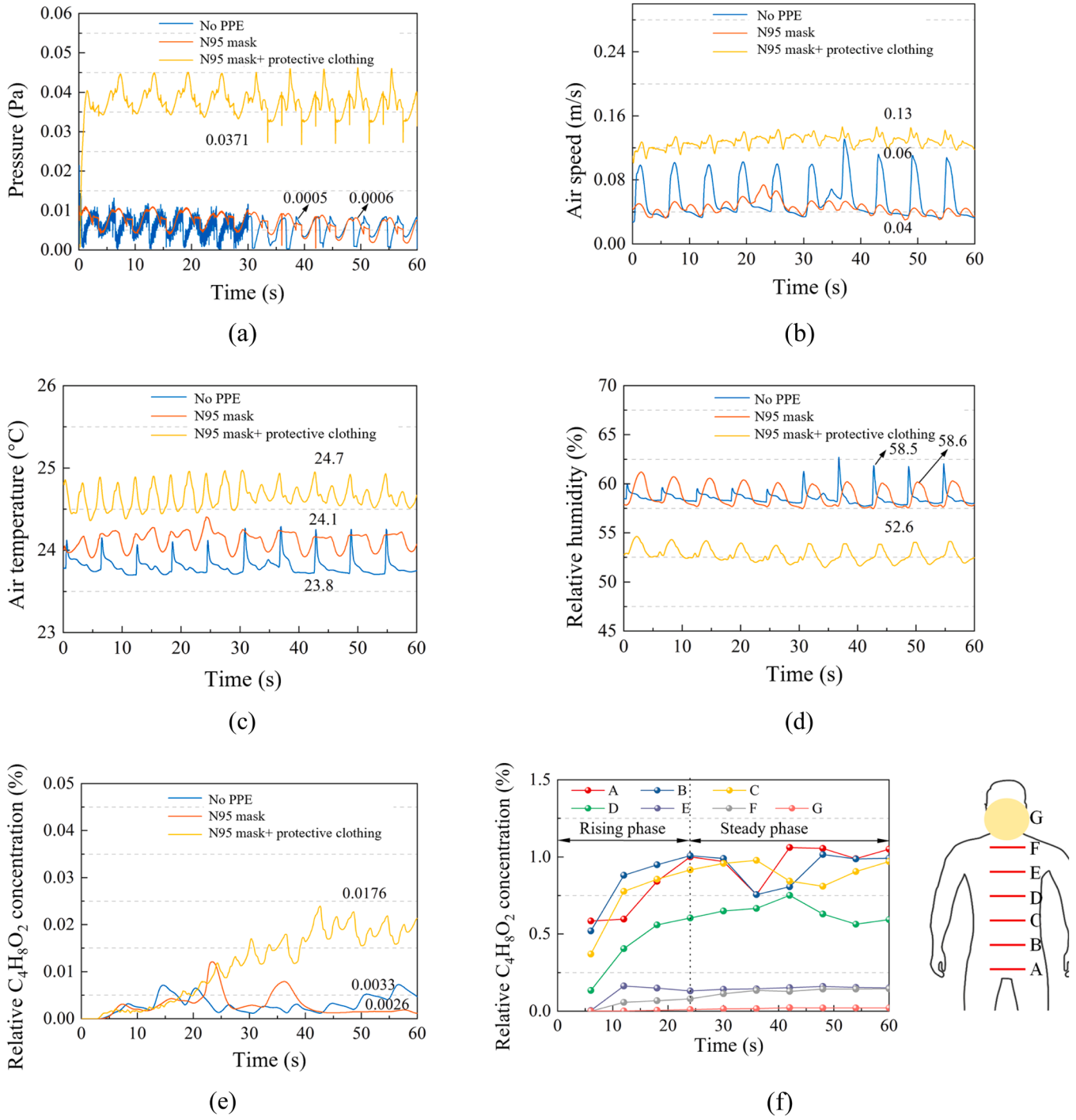


Fig. 6. Thermo-fluid parameters over time in the breathing zone (see Fig. 5) under different PPE usage conditions: (a) pressure, (b) air speed, (c) air temperature, (d) relative humidity, (e) relative $C_4H_8O_2$ concentration, and (f) distribution of $C_4H_8O_2$ emitted from the groin over time at different heights inside the PPE.

discomfort. Additionally, bio-effluent concentrations in the air layer between the skin and clothing increased remarkably. The leakage of bio-effluents from the neck opening demonstrates the limited effectiveness of protective clothing in controlling skin-emitted bio-effluents.

Fig. 8 visualizes the time-dependent spatial distribution of bio-effluents. At 6 s, most bio-effluents concentrated in the abdominal region, with only a small fraction reaching the breathing zone. By 12 s, bio-effluents accumulated on the chest. At 18 s, some bio-effluents spread along the arms. These patterns reveal progressive upward and lateral transport. By 30 s, bio-effluents leaked from both the neck and cuffs. The neck remained the dominant outlet. Cuffs acted as secondary leakage paths. At 60 s, high contaminant concentrations appeared in the breathing zone, posing risks to the surrounding clean environment and the wearer's breath health. This suggests that the bio-effluents accumulated inside the protective clothing, migrated upward, and ultimately escaped into the breathing zone through the neck opening, which explains the elevated contaminant levels near the face.

3.2. *Influence of PPE on inhalation exposure*

3.2.1. *Influence of breathing organ*

Fig. 9 illustrates the impact of breathing organs on inhalation

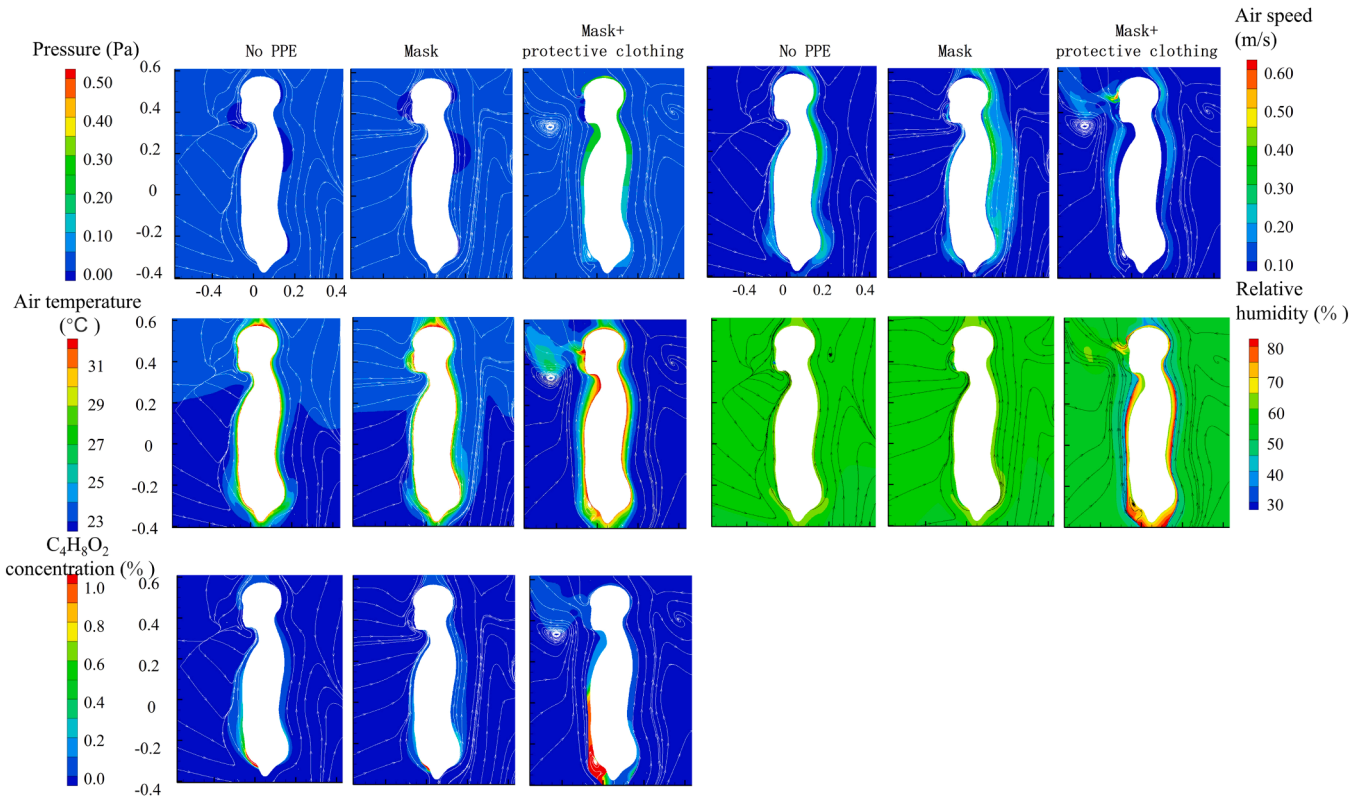


Fig. 7. Spatial distribution of different thermo-fluid parameters in the microenvironment around the human body under different PPE conditions on a vertical plane passing through the human body at 59 s.

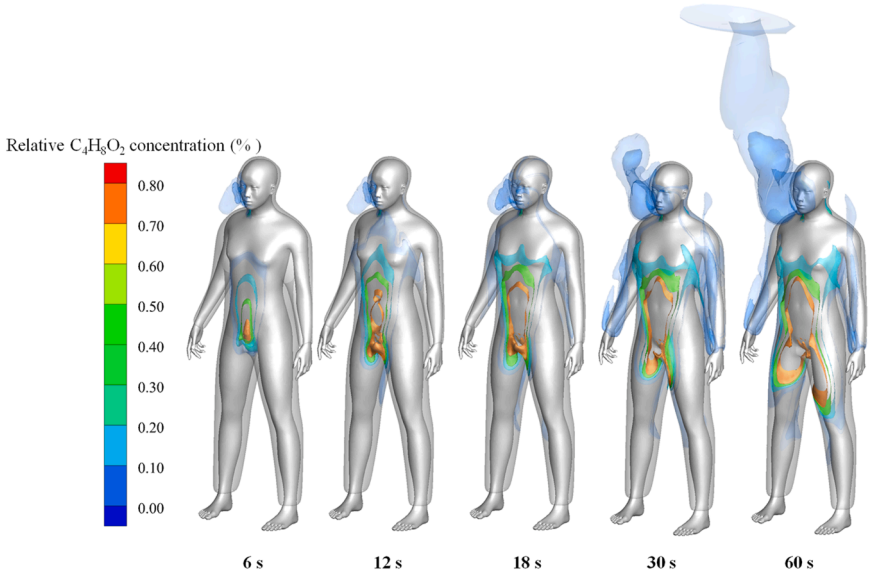


Fig. 8. Visualization of the spatial distribution of bio-effluents from the groin at different times.

exposure. Protective clothing increased inhalation exposure to skin-emitted bio-effluents, consistent with the results in Figs. 7 and 8. Relative inhalation concentration was slightly higher during nasal breathing than during oral breathing. This is primarily attributed to the fact that downward-facing nostrils allow greater intake of bio-effluents rising from lower body regions. Conversely, the relative exposure index showed a different trend. Oral breathing yielded a marginally higher index than nasal breathing. The discrepancy between these two metrics originated from the fact that, without PPE, skin bio-effluents emitted from the lower body move upwards along the body surface and are more easily inhaled through the nose than through the mouth.

3.2.2. *Influence of pulmonary ventilation rate*

Fig. 10 represents the influence of pulmonary ventilation rate on inhalation exposure. At low pulmonary ventilation rates (≤8 L/min), relative inhalation concentration (C^*) showed limited variation. A marked change appeared at a pulmonary ventilation rate of 9 L/min. Relative inhalation concentration increased substantially under this

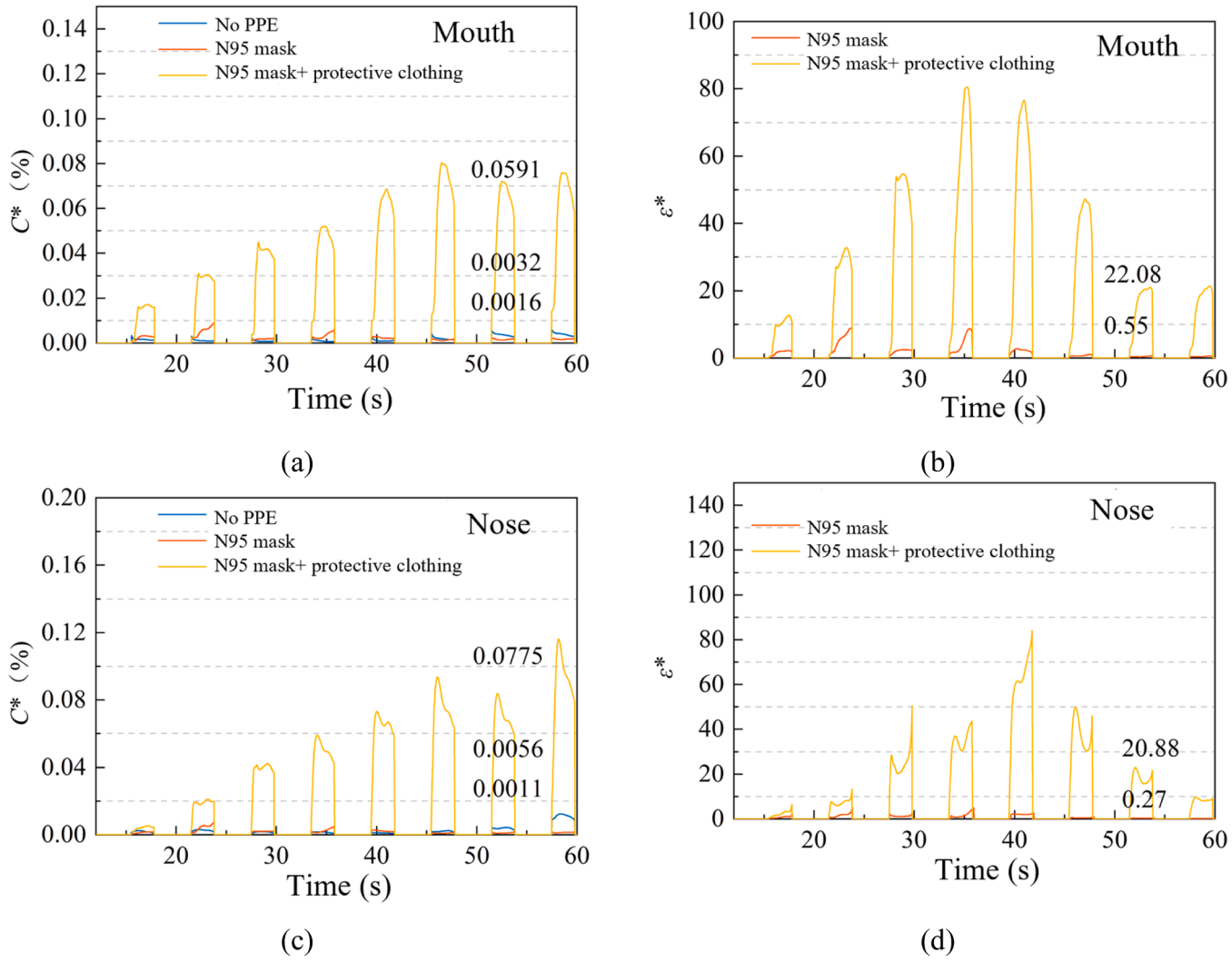


Fig. 9. Influence of breathing organ on inhalation exposure: (a) relative inhalation concentration: mouth, (b) relative exposure index: mouth, (c) relative inhalation concentration: nose, and (d) relative exposure index: nose.

condition. When the pulmonary ventilation rate increased from 6 L/min to 9 L/min, the relative inhalation concentration rose from 0.0591% to 0.0772%, an increase of 30.6%. Compared to the relative inhalation concentration, the relative exposure index (ε^*) increased by just 17.8%. This result confirms the sensitivity of inhalation exposure to activity intensity.

3.2.3. *Influence of emission rate*

Fig. 11 compares inhalation exposure under different skin contaminant emission rates. At low emission rates (70 and 700 μg $h^{-1}p^{-1}$), the relative inhalation concentration (C^*) remained nearly unchanged. However, at higher emission levels, both the relative inhalation concentration and the relative exposure index increased substantially, indicating greater accumulation inside PPE. For example, when the emission rate escalated from 700 μg $h^{-1}p^{-1}$ to 7000 μg $h^{-1}p^{-1}$, the relative inhalation concentration and relative exposure index increased by 35% and 43.6%, respectively. These results suggest that higher skin emission rates may pose an elevated risk of inhalation exposure.

3.2.4. *Influence of emission location*

Fig. 12 compares inhalation exposure from different emission locations. Bio-effluents emitted from the groin exhibited a higher relative inhalation concentration than those released from the armpit. The relative inhalation concentration reached 0.0591% for groin-emitted bio-effluents, compared to 0.0326% for armpit-emitted bio-effluents, representing an 81.3% increase over the armpit emission. Furthermore, the relative exposure index further highlighted this contract. Groin emissions yielded an index of 22.08, while armpit emissions produced a value of 8.59. This indicates that protective clothing more effectively suppresses the overflow of armpit bio-effluents into the breathing zone. Further analysis suggests that armpit effluents tend to travel along the arms and then leak out through the cuffs, making cuff leakage an important concern.

4. Discussion

4.1. *Modeling boundary conditions for PPE*

Most commercially available masks are made of soft materials, including nonwoven fabrics, such as meltblown polypropylene, and cotton [54]. Consequently, masks undergo deformation during actual use. Furthermore, mask designs vary widely across the market. Existing numerical studies often simplify mask geometry into smooth hemispherical surfaces [38,55], facial-sharp surfaces [36], or pleated facial-sharp surfaces [37,56,57]. The model employed in this study improves geometric fidelity compared with simplified shapes. However, deformation caused by breathing airflow is not considered, which may lead to discrepancies between numerical and experimental results. The

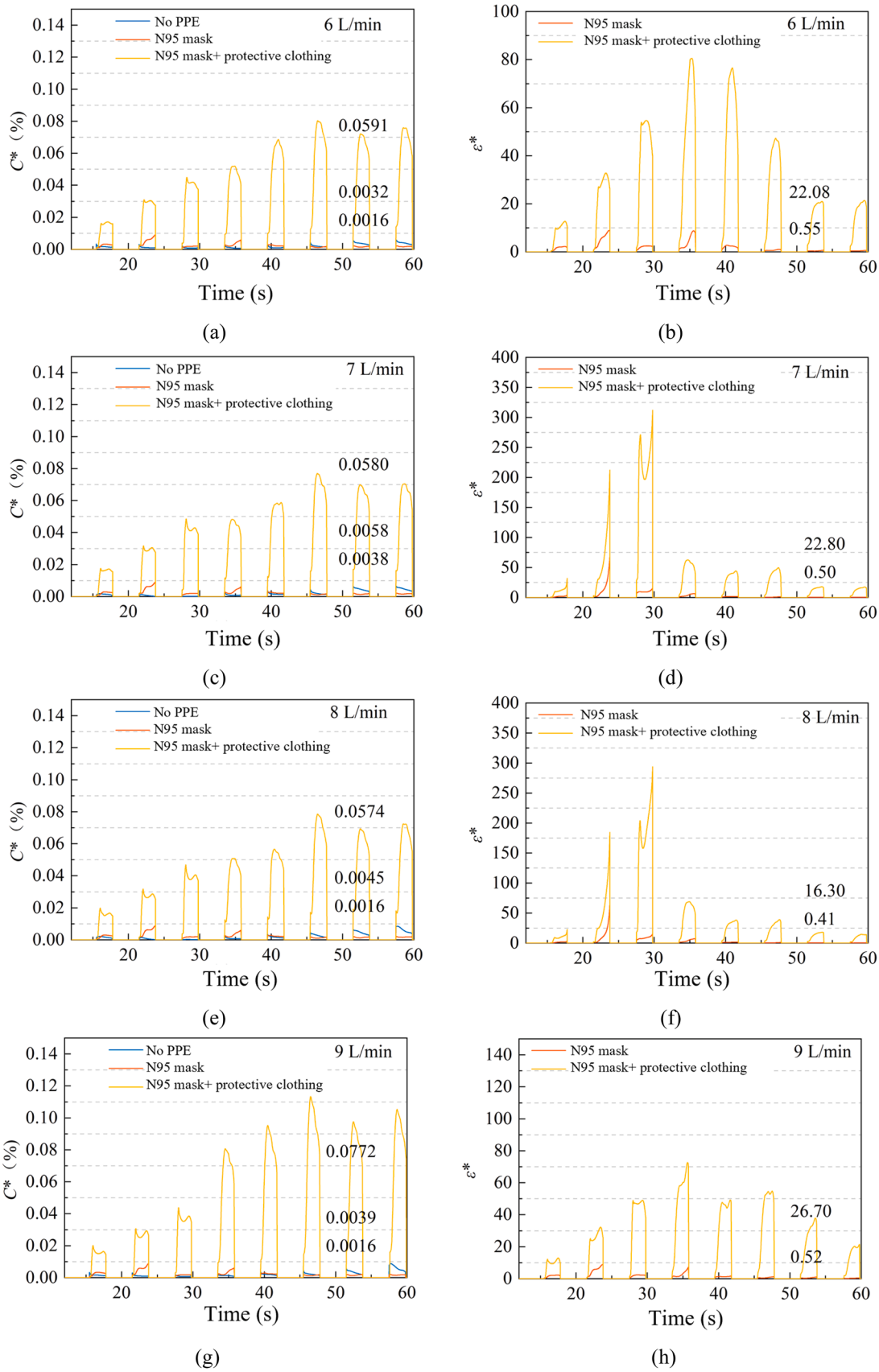


Fig. 10. Influence of pulmonary ventilation rate on inhalation exposure: (a) relative inhalation concentration: 6 L/min, (b) relative exposure index: 6 L/min, (c) relative inhalation concentration: 7 L/min, (d) relative exposure index: 7 L/min, (e) relative inhalation concentration: 8 L/min, (f) relative exposure index: 8 L/min, (g) relative inhalation concentration: 9 L/min and (h) relative exposure index: 9 L/min.

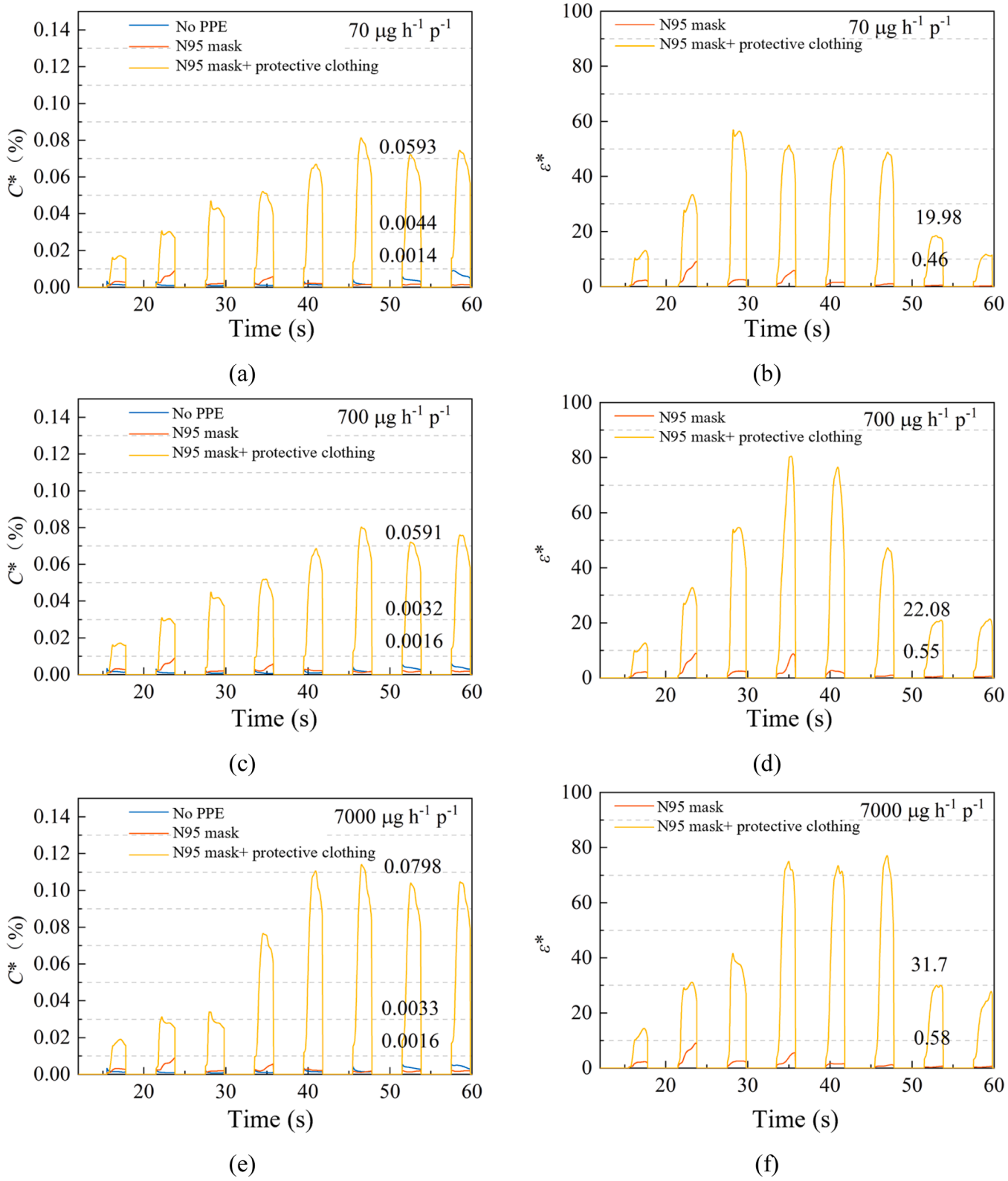


Fig. 11. Influence of emission rate on inhalation exposure: (a) relative inhalation concentration: 70 μg h^{-1} p^{-1}, (b) relative exposure index: 70 μg h^{-1} p^{-1}, (c) relative inhalation concentration: 700 μg h^{-1} p^{-1}, (d) relative exposure index: 700 μg h^{-1} p^{-1}, (e) relative inhalation concentration: 7000 μg h^{-1} p^{-1}, and (f) relative exposure index: 7000 μg h^{-1} p^{-1}.

influence of breathing-induced mask deformation on airflow and leakage paths warrants further investigation.

Except for masks, protective clothing is also made of soft materials. During use, protective clothing undergoes varying degrees of deformation, which affects the thickness of the air layer between the clothing and the skin. This deformation may also alter the breathability of the material. Body movement further increases modelling complexity by dynamically changing the thickness of the air gap. These interactions

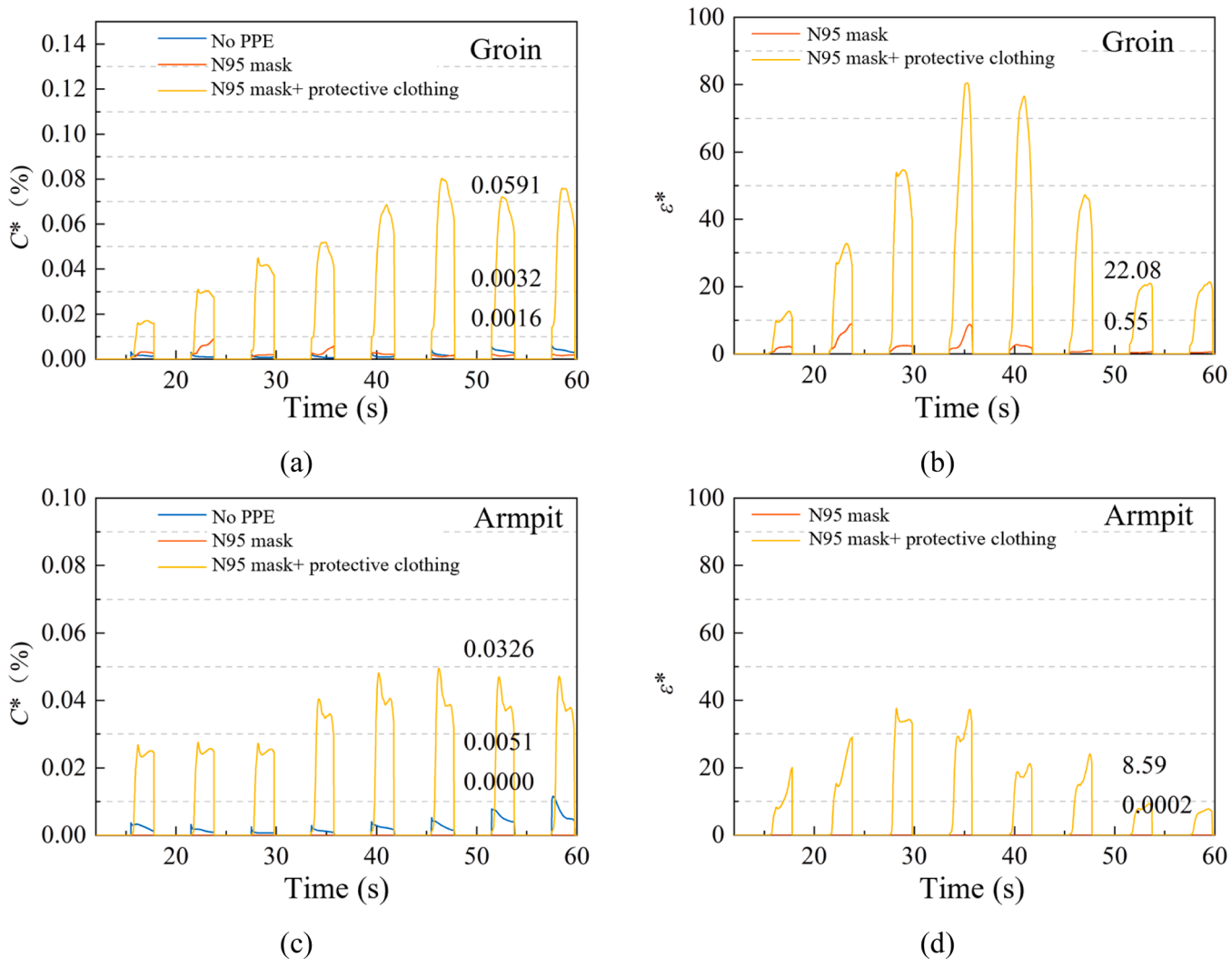


Fig. 12. Influence of emission location on inhalation exposure: (a) relative inhalation concentration: groin, (b) relative exposure index: groin, (c) relative inhalation concentration: armpit, and (d) relative exposure index: armpit.

complicate accurate numerical representations. Currently, research focusing exclusively on protective clothing modeling remains limited. Some researchers have reported the range of thickness of air gap, such as 5–37 mm [39] and 5–25 mm [40], for ordinary clothing. The air gap dimensions used in this study align well with previously reported measurements. Despite this consistency, static models used in this study cannot fully represent real human motion. Dynamic mesh-based simulation techniques for PPE remain an important research direction.

Airflow modelling in porous filtration materials generally follows either direct approaches [58] or indirect approaches [45,59]. The direct approach explicitly models actual geometric shapes with microporous structures, which requires high computational costs. Most mask simulations employed indirect methods based on porous media models. These models replace complex microstructures with equivalent resistance parameters. This strategy balances accuracy and computational efficiency. In our previous studies [15,36], common commercial masks were experimentally tested, and the flow resistance coefficients were then determined for numerical simulations. In this study, the same parameters were used in the present study. Compared to masks, protective clothing exhibits much higher filtration resistance, so air permeation through protective clothing was excluded in the present research. This assumption reflects its limited breathability. Given the large impact of protective clothing on the microenvironment surrounding the human body, refining the protective clothing model deserves further investigation when evaluating the inhalation exposure of users.

4.2. *Validation of personal protective equipment modeling*

Validation is particularly critical for numerical simulations. However, many previous PPE studies used indoor room-scale airflow data without PPE to validate the flow field around the human body. Such approaches overlook PPE-induced microenvironment changes. PPE alters airflow, heat transfer, and contaminant transport near the human body. Indoor-scale parameters without PPE cannot fully represent these effects. Therefore, the validity of numerical models under PPE conditions requires focused examination. In this study, the mask model has been scientifically validated in our studies [36], primarily including: (1) the attenuation of exhaled airflow after passing through the mask, (2) the decay of exhaled contaminant concentration after passing through the mask, and (3) the visualization of leakage through the gap around the mask. These provide a relatively comprehensive support for accurate mask simulation. However, quantitative data to validate leakage at mask edges remains limited. This gap restricts complete validation. Experimental validation for protective clothing is even more limited. Few studies report detailed internal microenvironment parameters. Reliable validation data remains scarce. This study validates clothing simulation by comparing contaminant concentrations inside and outside the protective clothing. The approach provides indirect evidence of internal

transport behavior. Differences between real clothing shape and numerical models may still influence airflow and contaminant distribution.

Comprehensive validation of mask simulations should address three aspects, including edge leakage, surface permeation, and the internal mask cavity environment. These parameters can be obtained using various experimental methods. Human subject experiments capture realistic breathing and mask fit. However, their repeatability is limited since subjects struggle to maintain fixed postures for extended periods. Future studies may incorporate human subject experiments to further validate inhalation exposure and bio-effluent transport predicted by the CFD model under realistic wearing conditions. Thermal manikin experiments provide stable, controllable conditions. While they simplify testing but deviate from real human behavior. Wearable micro-sensor technology offers a promising approach for validating protective clothing. It enables multi-point monitoring inside the clothing, improving data richness. Three-dimensional scanning technology can capture realistic clothing geometry. This method provides high modelling accuracy, which should be reflected in these measurements. This combination enables posture-specific numerical modelling and enhances simulation accuracy. Overall, experimental databases for validating combined mask and protective clothing models remain insufficient. Expanding these datasets will strengthen further simulations.

4.3. Transport characteristics of bio-effluents in personal protective equipment

Exhaled bio-effluents predominantly accumulate inside the mask cavity. Relative carbon dioxide concentrations inside the mask can reach 29–54%, indicating a high potential risk of inhalation exposure [15,33]. Compared to breath bio-effluents, skin-emitted bio-effluents would escape more easily since protective clothing has larger leakage openings than masks. This structural difference facilitates the outward transport of skin bio-effluents. The findings of this study indicate that the relative concentrations of bio-effluents inside the protective clothing range from 0.02% to 0.60%. Bio-effluent concentration decreases vertically along the body. This gradient reflects the upward contaminant transport. The relative concentration reaches 0.6% near the chest, 0.2% at the neck, and 0.018% in the breathing zone.

When protective clothing is worn, the concentration of skin bio-effluents in the breathing zone increases markedly. The relative concentration of skin bio-effluents increases by approximately 5.3 times without PPE. This rise highlights the exposure effects of clothing-induced confinement. Earlier studies [21,60] used a breathing thermal manikin to assess exposure under ordinary clothing. Protective clothing offers higher sealing performance than ordinary garments. This feature enables skin bio-effluents to accumulate longer within the internal air layer before being diluted. A distinct pressure difference develops between the interior and exterior of the protective suit, driving bio-effluents upwards. Consequently, PPE use increases the concentration of self-generated bio-effluents in the breathing zone. However, activity intensity and posture may further alter the pressure differential between the inside and outside of the protective clothing, thereby influencing the dispersion of these bio-effluents. Additionally, PPE size and form affect the microenvironment around the body, thereby modifying dispersion patterns, which warrant further investigation. Furthermore, material properties such as breathability, fabric permeability, and moisture accumulation can also influence airflow patterns and contaminant retention within PPE. Variations in these properties among different protective clothing types may modify local bio-effluent concentrations, alter the development of thermal plumes, and impact leakage paths. Future studies should consider these factors to better quantify how material variability and humidity affect inhalation exposure under realistic PPE conditions.

4.4. Effect of PPE on inhalation exposure

Wearing respiratory protective equipment can result in an inhalation fraction of exhaled bio-effluents of up to 60%, greatly exceeding the 1% observed without PPE [61]. Oxygen content in inhaled air decreases by approximately 14.3% during PPE use. Previous studies [62,63] have investigated mask-related inhalation exposure, with Law et al. [62] reporting a 7.4% increase in end-tidal carbon dioxide and Lee et al. [63] observing a 37% reduction in inspiratory and expiratory volumes with N95 masks. These findings suggest potential discomfort and health impacts from respiratory protection, particularly among healthcare and occupational workers engaged in high-intensity activities and prolonged mask use. Reported adverse symptoms include dizziness, headaches, drowsiness, and elevated heart rate [10,64,65]. These symptoms may result from a disrupted balance between carbon dioxide (CO_2) and oxygen (O_2), leading to hypercapnia (elevated blood CO_2) and/or hypoxemia (reduced blood O_2 levels). In addition, skin-emitted bio-effluents accumulate in the breathing zone, with relative inhalation concentration and relative exposure index ranging from 0.03% and 8.6 to 0.08% and 31.7, respectively, which are considerably higher than those without PPE. Although the absolute concentrations of skin-emitted bio-effluents are relatively low, their potential health implications should not be considered negligible. Long-term exposure, cumulative inhalation, and the formation of secondary reaction products could still pose risks, particularly for individuals wearing PPE for extended periods, such as during surgeries or prolonged cleanroom operations. These factors have not been fully quantified in the present study, and further investigations, including longer-duration simulations and measurements under realistic working conditions, are needed to assess potential health effects more comprehensively.

4.5. Limitations and further research direction

Several limitations of this study should be acknowledged. Firstly, this study employed a static, fixed posture using a manikin-based simulation, which does not capture realistic body movements during PPE use. Under higher metabolic rates associated with moderate to high-intensity activities, changes in heat generation, pulmonary ventilation, body posture, and PPE fit may occur, thereby altering the internal microenvironment and contaminant transport. PPE deformation and body motion can also influence the thickness of the air layer and local pressure differences, affecting the dispersion of bio-effluents and subsequent inhalation exposure. Furthermore, the validation in this study is model-based, relying on controlled manikin experiments. While room conditions were found to have minimal effect on contaminant transport inside the PPE, significant physical differences remain between human subjects and manikins. Therefore, future research should incorporate dynamic manikins and human subject experiments (e.g., using tracer gas or wearable sensors) to better represent realistic scenarios and further validate CFD-predicted inhalation exposure under actual conditions of PPE use. T. Secondly, this study assumed a thermally comfortable indoor environment. The air temperature and relative humidity were kept within a narrow range. The simulations considered a light-activity scenario typical of PPE use in environments such as clean rooms or operating rooms under thermally comfortable conditions, where sweating is generally limited. Constant temperatures were assigned to different body segments, allowing thermal effects to be represented without explicitly coupling a thermoregulation model. These parameters can affect the development of thermal plumes around the human body, potentially enhancing or weakening pollutant transport upward. In addition, sweating and latent heat loss may still influence the microclimate between the body and PPE, particularly water vapor content, potentially affecting bio-effluent transport and inhalation exposure. Future studies should therefore consider coupling CFD with a thermoregulation model to better represent segmental sensible and latent heat losses. The environmental effects of exposure deserve further

exploration. Thirdly, the capacity to remove indoor bio-effluents is determined by indoor air distribution, such as ventilation patterns and rate. This study employed a low indoor ventilation rate. Further research should integrate optimized airflow organization with PPE to more effectively control human-related bio-effluents. Finally, a simplified breathing cycle with a short pause between exhalation and inhalation was adopted in the simulations. However, breathing patterns vary among individuals and activity levels, which may influence airflow dynamics and inhalation exposure in the breathing zone.

5. Conclusions

This study developed a suite of realistic-sharp personal protective equipment, including a mask and protective clothing. A scientifically validated numerical model was then applied to examine factors influencing inhalation exposure to self-emitted bio-effluents. The following conclusions can be drawn:

(1) Wearing protective clothing altered the thermal-fluid parameters both inside the PPE and in the breathing zone. The average air temperature in the breathing zone increased by 0.9 °C, and the average air speed increased by 0.09 m/s compared with no protective clothing.
(2) Protective clothing use formed a pressure difference between its interior and exterior, which drove skin bio-effluents upward along the body and into the breathing zone. Leakage mainly occurred at the neck and cuffs. The relative concentration of bio-effluents in the breathing zone increased from 0.0033% to 0.0176%, indicating a potential increased inhalation exposure risk.
(3) Wearing protective clothing increased the relative inhalation concentration of skin bio-effluents. Nasal breathing resulted in slightly higher inhalation concentrations than oral breathing due to different transport pathways. Compared to unclothing, PPE use increased inhalation exposure during oral breathing more than during nasal breathing, indicating that breathing mode modifies PPE-related exposure effects.
(4) Increasing pulmonary ventilation rates resulted in larger inhalation exposure. When the pulmonary ventilation rate increased from 6 L/min to 9 L/min under a standing posture and oral breathing, the relative inhalation concentration and relative exposure index increased by 30.6% and 17.8%, respectively, indicating that high-intensity activity increases the inhalation exposure to skin-emitted bio-effluents.
(5) Low emission rate of skin bio-effluents had a limited influence on inhalation exposure. As the emission rate exceeded 700 $\mu g\ h^{-1}p^{-1}$, the inhalation exposure greatly increased. When the emission rate escalated from 700 $\mu g\ h^{-1}p^{-1}$ to 7000 $\mu g\ h^{-1}p^{-1}$ under a standing posture and oral breathing, the relative inhalation concentration and relative exposure index increased by 35% and 43.6%, respectively.
(6) Bio-effluents emitted from the groin exhibited a higher inhalation exposure than those released from the armpit. Under a standing posture, oral breathing, the relative inhalation concentration and relative exposure index of bio-effluents emitted from the groin were 1.81 and 2.57 times higher than those from the armpit. This indicates that protective clothing more effectively restricts armpit bio-effluents from entering the breathing zone.

From a practical perspective, these results suggest that leakage control at the neck and cuffs should be prioritized in PPE design and usage, as these locations serve as dominant transport pathways for skin-emitted bio-effluents. In addition, the groin region should be considered a key emission hotspot due to its higher potential to contribute to inhalation exposure. Improving sealing performance and airflow management around these critical regions may help reduce exposure risks for PPE wearers.

CRediT authorship contribution statement

Zhongjian Jia: Writing – original draft, Visualization, Validation, Software, Methodology, Investigation, Formal analysis, Data curation. **Zhengtao Ai:** Writing – review & editing, Supervision, Resources, Project administration, Methodology, Funding acquisition, Conceptualization. **Xiaochen Zhang:** Visualization, Methodology, Investigation. **Zhengxuan Liu:** Writing – review & editing, Methodology. **Lexuan Zhong:** Writing – review & editing.

Declaration of competing interest

The authors declare that they have no known competing financial interests or personal relationships that could have appeared to influence the work reported in this paper.

Acknowledgement

This study was supported by the Fundamental Research Funds for the Central Universities (No. 531118010378).

Data availability

Data will be made available on request.

References

[1] A. Tabah, M. Ramanan, K.B. Laupland, et al., Personal protective equipment and intensive care unit healthcare worker safety in the COVID-19 era (PPE-SAFE): an international survey, J. Crit. Care 59 (2020) 70–75.
[2] M. Holland, D.J. Zaloga, C.S. Friderici, COVID-19 Personal protective equipment (PPE) for the emergency physician, Vis. J. Emerg. Med. (2020) 100740.
[3] R. Chen, A. Shiue, J. Liu, et al., Integrated on-site collection and off-site analysis of airborne molecular contamination in cleanrooms for integrated circuit manufacturing processes, Build. Environ. 214 (2022) 108941.
[4] C.J. Kahler, R. Hain, Fundamental protective mechanisms of face masks against droplet infections, J. Aerosol. Sci. 148 (2020) 105617.
[5] Z. Jia, Z. Zhang, Z. Ai, Adverse reactions of workers to the use of personal protective equipment in pharmaceutical factories: a cross-sectional survey, Energy Built Environ. (2025).
[6] H. Jiang, B. Cao, Y. Zhu, Improving thermal comfort of individuals wearing medical protective clothing: two personal cooling strategies integrated with the polymer water-absorbing resin material, Build. Environ. 243 (2023) 110730.
[7] S.Y. Kyung, Y. Kim, H. Hwang, et al., Risks of N95 face mask use in subjects with COPD, Respir. Care 65 (5) (2020) 658–664.
[8] E. Jafari, M. Togha, H. Kazemizadeh, et al., Evaluation of headache associated with personal protective equipment during COVID-19, Brain Behav. 11 (12) (2021) e2435.
[9] X. Zhang, P. Wargocki, Z. Lian, et al., Effects of exposure to carbon dioxide and bioeffluents on perceived air quality, self-assessed acute health symptoms, and cognitive performance, Indoor Air 27 (1) (2017) 47–64.
[10] P. Sukul, J. Bartels, P. Fuchs, et al., Effects of COVID-19 protective face masks and wearing durations on respiratory haemodynamic physiology and exhaled breath constituents, Eur. Respir. J. 60 (3) (2022) 2200009.
[11] N. Wang, L. Ernle, G. Bekö, P. Wargocki, J. Williams, Emission rates of volatile organic compounds from humans, Environ. Sci. Technol. 56 (8) (2022) 4838–4848.
[12] Z. Zou, J. He, X. Yang, An experimental method for measuring VOC emissions from individual human whole-body skin under controlled conditions, Build. Environ. 181 (2020) 107137.
[13] Z. Zou, X. Yang, Volatile organic compound emissions from the human body: decoupling and comparison between whole-body skin and breath emissions, Build. Environ. 226 (2022) 109713.
[14] Z. Jia, Z. Zhang, H. Tan, J. Chen, L. Zhu, L. Wang, W. Tan, Z. Ai, Characterizing volatile organic compounds from personal protective equipment users: implications to cleanroom air quality and occupational health, J. Hazard. Mater. 495 (2025) 138938.
[15] Z. Jia, Z. Ai, G. Bekö, The use of respiratory protective equipment redefines breathing zone and increases inhalation exposure of self-exhaled pollutants, Build. Environ. 247 (2024) 111035.
[16] L. Dormont, J.M. Bessiere, A. Cohuet, Human skin volatiles: a review, J. Chem. Ecol. 39 (5) (2013) 569–578.
[17] B.D. Costello, A. Amann, H. Al-Kateb, et al., A review of the volatiles from the healthy human body, J. Breath. Res. 8 (1) (2014) 014001.
[18] X. Sun, VOC Emission from Humans and the Interactions Between Humans and the Environment, Tsinghua University, 2017. Chinese.

[19] C. Arata, N. Heine, N. Wang, et al., Heterogeneous ozonolysis of squalene: gas-phase products depend on water vapor concentration, Environ. Sci. Technol. 53 (24) (2019) 14441–14448.
[20] O.S.a.H. Administration, Enforcement Guidance For Personal Protective Equipment in General Industry (OSHA Instruction CPL 02-01-050), in: U.S.D.o. Labor (Ed.) 2011.
[21] M. Bivolarova, W. Kierat, E. Zavrl, et al., Effect of airflow interaction in the breathing zone on exposure to bio-effluents, Build. Environ. 125 (nov) (2017) 216–226.
[22] Z. Jia, Z. Ai, Face shield intensifies inhaled exposure to self-generated bio-effluents, Build. Environ. 217 (2022) 109070.
[23] M.S. Waring, J.R. Wells, Volatile organic compound conversion by ozone, hydroxyl radicals, and nitrate radicals in residential indoor air: magnitudes and impacts of oxidant sources, Atmos. Environ. 106 (2015) 382–391.
[24] R. Bhoonah, M. Mendez, A. Maury-Micolier, Human health impacts and indoor chemical reactions of VOCs from cleaning products and occupants, Atmos. Environ. 338 (2024) 120846.
[25] G. Morantes, B. Jones, C. Molina, et al., Harm from residential indoor air contaminants, Environ. Sci. Technol. 58 (1) (2024) 242–257.
[26] J. Zeng, M. Mekic, X. Xu, et al., A novel insight into the ozone–skin lipid oxidation products observed by secondary electrospray ionization high-resolution mass spectrometry, Environ. Sci. Technol. 54 (21) (2020) 13478–13487.
[27] B.K. Coleman, H. Destaillats, A.T. Hodgson, et al., Ozone consumption and volatile byproduct formation from surface reactions with aircraft cabin materials and clothing fabrics, Atmos. Environ. 42 (4) (2008) 642–654.
[28] A.C. Rai, B. Guo, C.-H. Lin, et al., Ozone reaction with clothing and its initiated particle generation in an environmental chamber, Atmos. Environ. 77 (2013) 885–892.
[29] S. Zhu, S. Kato, S. Murakami, T. Hayashi, Study on inhalation region by means of CFD analysis and experiment, Build. Environ. 40 (10) (2005) 1329–1336.
[30] K. Kuga, P. Wargocki, K. Ito, Breathing zone and exhaled air re-inhalation rate under transient conditions assessed with a computer-simulated person, Indoor Air 32 (2) (2022) e13003.
[31] J. Zong, Z. Ai, G. Ma, Accurate evaluation of inhalation exposure based on CFD predicted concentration in the breathing zone towards personalized and smart control, J. Build. Eng. 71 (2023) 106404.
[32] Z. Lei, J. Yang, Computing carbon dioxide and humidity in filtering facepiece respirator cavity during breathing cycles, 2014.
[33] Z. Jia, Z. Ai, Z. Zhang, C.M. Mak, H.Ming Wong, A mathematical model for accurately predicting face mask wearer's inhalation exposure to self-exhaled and external pollutants, Sep. Purif. Technol. 336 (2024) 126312.
[34] J. Gupta, C.-H. Lin, C. Qi, Characterizing exhaled airflow from breathing and talking, Indoor. Air. 20 (2009) 31–39.
[35] Z.T. Ai, A.K. Melikov, Airborne spread of expiratory droplet nuclei between the occupants of indoor environments: a review, Indoor. Air. 28 (4) (2018) 500–524.
[36] Z. Jia, Z. Ai, X. Yang, et al., Towards an accurate CFD prediction of airflow and dispersion through face mask, Build. Environ. 229 (2023) 109932.
[37] T. Dbouk, D. Drikakis, On respiratory droplets and face masks, Phys. Fluids 32 (6) (2020) 063303.
[38] A. Khosronejad, C. Santoni, K. Flora, et al., Fluid dynamics simulations show that facial masks can suppress the spread of COVID-19 in indoor environments, AIP. Adv. 10 (12) (2020) 125109.
[39] E. Mert, A. Psikuta, M.-A. Bueno, et al., The effect of body postures on the distribution of air gap thickness and contact area, Int. J. Biometeorol. 61 (2) (2017) 363–375.
[40] A. Joshi, A. Psikuta, M.-A. Bueno, et al., Effect of movement on convection and ventilation in a skin-clothing-environment system, Int. J. Thermal Sci. 166 (2021) 106965.
[41] A. Joshi, A. Psikuta, S. Annaheim, et al., Modelling of heat and mass transfer in clothing considering evaporation, condensation, and wet conduction with case study, Build. Environ. 228 (2023) 109786.
[42] H. Shen, Y. An, H. Zhang, et al., 3D numerical investigation of the heat and flow transfer through cold protective clothing based on CFD, Int. J. Heat. Mass Transf. 175 (2021) 121305.
[43] Z. Kang, D. Shou, J. Fan, Numerical modeling of body heat dissipation through static and dynamic clothing air gaps, Int. J. Heat. Mass Transf. 157 (2020) 119833.
[44] M. Bivolarova, W. Kierat, E. Zavrl, Z. Popiolek, A. Melikov, Effect of airflow interaction in the breathing zone on exposure to bio-effluents, Build. Environ. 125 (2017) 216–226.
[45] H. Salati, M. Khamooshi, S. Vahaji, et al., N95 respirator mask breathing leads to excessive carbon dioxide inhalation and reduced heat transfer in a human nasal cavity, Phys. Fluids 33 (8) (2021) 081913.
[46] C. Yang, X. Yang, B. Zhao, The ventilation needed to control thermal plume and particle dispersion from manikins in a unidirectional ventilated protective isolation room, Build. Simul. (2015) 551–565.
[47] Z. Jia, Z. Ai, S. Cao, et al., Effectiveness of respiratory protective equipment on source control of exhaled pollutants, J. Build. Eng. 86 (2024) 108742.
[48] Y. Xu, X. Luo, Y. Xia, et al., Dynamic coordinated air supply for moving individuals in industrial settings: effectiveness evaluation and demonstration, Build. Environ. 263 (2024) 111873.
[49] A.K. Melikov, R. Cermak, M. Majer, Personalized ventilation: evaluation of different air terminal devices, Energy Build. 34 (8) (2002) 829–836.
[50] N. Gao, J. Niu, H. Zhang, Coupling CFD and human body thermoregulation model for the assessment of personalized ventilation, HVAC&R. Res. 12 (3) (2006) 497–518.
[51] C. Zhang, P.V. Nielsen, L. Liu, et al., The source control effect of personal protection equipment and physical barrier on short-range airborne transmission, Build. Environ. 211 (2022) 108751.
[52] D.H. Bennett, T.E. McKone, J.S. Evans, et al., Defining intake fraction, Environ. Sci. Technol. 36 (9) (2002) 207–211.
[53] J.S. Russo, E. Khalifa, Computational study of breathing methods for inhalation exposure, HVAC&R. Res. 17 (4) (2011) 419–431.
[54] L.H. Kwong, R. Wilson, S. Kumar, et al., Review of the breathability and filtration efficiency of common household materials for face masks, ACS. Nano 15 (4) (2021) 5904–5924.
[55] A. Khosronejad, S. Kang, F. Wermelinger, et al., A computational study of expiratory particle transport and vortex dynamics during breathing with and without face masks, Phys. Fluids 33 (6) (2021) 066605.
[56] J. Xi, K. Barari, X.A. Si, et al., Inspiratory leakage flow fraction for surgical masks with varying gaps and filter materials, Phys. Fluids 34 (4) (2022) 041908.
[57] T. Solano, C. Ni, R. Mittal, et al., Perimeter leakage of face masks and its effect on the mask's efficacy, Phys. Fluids 34 (2022) 051902.
[58] A.M. Aliyu, D. Singh, C. Uzoka, R. Mishra, Dispersion of virus-laden droplets in ventilated rooms: effect of homemade facemasks, J. Build. Eng. 44 (2021) 102933.
[59] X. Zhang, L. Hui, S. Shen, et al., Investigation of the flow-field in the upper respiratory system when wearing N95 filtering facepiece respirator, J. Occup. Environ. Hyg. 13 (5) (2015) 372–382.
[60] W. Kierat, M. Bivolarova, E. Zavrl, Z. Popiolek, A. Melikov, Accurate assessment of exposure using tracer gas measurements, Build. Environ. 131 (2018) 163–173.
[61] K. Kuga, P. Wargocki, K. Ito, Breathing zone and exhaled air re-inhalation rate under transient conditions assessed with a computer-simulated person, Indoor. Air. 32 (2) (2022) 13003.
[62] C.S. Law, P.S. Lan, G.H. Glover, Effect of wearing a face mask on fMRI BOLD contrast, Neuroimage 229 (2021) 117752.
[63] H.P. Lee, D.Y. Wang, Objective assessment of increase in breathing resistance of N95 respirators on human subjects, Ann. Occup. Hygiene 55 (8) (2011) 917–921.
[64] C. Liu, G. Li, Y. He, et al., Effects of wearing masks on human health and comfort during the COVID-19 pandemic, IOP Conf. Series (2020) 012034.
[65] M. Deng, X. Wang, C.C. Menassa, Investigating the effect of wearing masks on office work in indoor environments during a pandemic using physiological sensing, Build. Environ. 221 (2022) 109346.